

Anisotropic contribution to the van der Waals and the Casimir-Polder energies for CO₂ and CH₄ molecules near surfaces and thin films

Priyadarshini Thiyam,^{1,*} Prachi Parashar,^{2,3,†} K. V. Shajesh,^{2,‡} Clas Persson,^{1,4,5} Martin Schaden,⁶ Iver Brevik,⁷ Drew F. Parsons,⁸ Kimball A. Milton,³ Oleksandr I. Malyi,^{5,§} and Mathias Boström^{5,||}

¹*Department of Materials Science and Engineering, Royal Institute of Technology, SE-100 44 Stockholm, Sweden*

²*Department of Physics, Southern Illinois University–Carbondale, Carbondale, Illinois 62901, USA*

³*Homer L. Dodge Department of Physics and Astronomy, University of Oklahoma, Norman, Oklahoma 73019, USA*

⁴*Department of Physics, University of Oslo, P.O. Box 1048 Blindern, NO-0316 Oslo, Norway*

⁵*Centre for Materials Science and Nanotechnology, University of Oslo, P.O. Box 1048 Blindern, NO-0316 Oslo, Norway*

⁶*Department of Physics, Rutgers, The State University of New Jersey, Newark, New Jersey 07102, USA*

⁷*Department of Energy and Process Engineering, Norwegian University of Science and Technology, NO-7491 Trondheim, Norway*

⁸*School of Engineering and IT, Murdoch University, 90 South St, Murdoch, WA 6150, Australia*

(Received 1 June 2015; revised manuscript received 5 October 2015; published 5 November 2015)

In order to understand why carbon dioxide (CO₂) and methane (CH₄) molecules interact differently with surfaces, we investigate the Casimir-Polder energy of a linearly polarizable CO₂ molecule and an isotropically polarizable CH₄ molecule in front of an atomically thin gold film and an amorphous silica slab. We quantitatively analyze how the anisotropy in the polarizability of the molecule influences the van der Waals contribution to the binding energy of the molecule.

DOI: [10.1103/PhysRevA.92.052704](https://doi.org/10.1103/PhysRevA.92.052704)

PACS number(s): 34.20.Cf, 42.50.Lc, 71.15.Mb

I. INTRODUCTION

The van der Waals force, and more generally, the Casimir-Polder force are topics of considerable interest in a wide range of interdisciplinary subjects from pure to applied sciences [1]. These forces describe the interaction between two neutral polarizable objects in nonretarded and retarded limits, respectively. They could play an important role in nanoscale devices [2,3], stability of trapped Bose-Einstein condensate [4,5], dynamical Casimir effect and friction [6–10], surface adsorption [11], etc. For a more comprehensive view of the subject see [1,12,13].

In this paper we shall investigate the anisotropic characteristic of the van der Waals and the Casimir-Polder interactions, which has precursors going back to Axilrod and Teller in 1943 [14], and Craig and Power in 1969 [15,16]. The anisotropic polarizabilities of the interacting objects lead to preferential orientation of the atom or molecule above the surface. This could play a significant role in preferential adsorption of the molecules such as carbon dioxide (CO₂) and methane (CH₄) [17,18].

From previous studies [19,20] we know that an isotropically averaged CO₂ molecule and an isotropic CH₄ molecule adhere to surfaces with very similar van der Waals energies. In the present paper we generalize this by developing a formalism to include the effect of anisotropic properties of the atom or molecule interacting with the perpendicularly anisotropic surface (see Fig. 1). This has been partially addressed earlier in [21,22].

The arrangement of the electron cloud in a CH₄ molecule is such that overall it has zero static dipole moment. This means that in a uniform electric field the molecule has no preferred orientation, and the induced dipole is simply formed parallel to the electric field. That is, the polarizability tensor for CH₄ is isotropic even though the molecule is not spherical. The nonsphericity of the molecule is expressed as anisotropy in higher order polarizability tensors (quadrupole, octupole, etc.). A CO₂ molecule, on the other hand, is linearly polarizable. In particular, we study the contribution from anisotropic polarizabilities to the Casimir-Polder interaction energy of a CO₂ and a CH₄ molecule in front of an atomically thin gold film and an amorphous silica slab. We choose an isotropic surface (amorphous silica) and an anisotropic surface (gold) in order to study the effect of anisotropy of the surface on the interaction as well. The dielectric function of amorphous silica is calculated using density functional theory (DFT). For gold, we explore the data of the dielectric function available in Ref. [23] also based on DFT. The dielectric function data of gold films of different thicknesses available in this reference facilitate the study of the variation of the interaction energy with film thickness.

In Sec. II, we present the formalism of the Casimir-Polder interaction energy between a completely anisotropic molecule and a dielectric slab which is anisotropic in the direction perpendicular to the surface. In Sec. III, we briefly summarize the method used for the calculation of the dielectric properties of the slabs. We also briefly describe the procedure used to obtain the anisotropic polarizabilities of the molecules. The anisotropic polarizabilities of CO₂ and CH₄ molecules are obtained from *ab initio* calculations [24,25]. Together the dielectric properties thus obtained are used to determine how the difference in the nature of polarizabilities of CO₂ and CH₄ distinguish their interaction energies near a surface. We present our results in Sec. IV, and end with a few conclusions in Sec. V.

*thiyam@kth.se

†prachi@nhn.ou.edu

‡kvshajesh@gmail.com

§oleksandr.malyi@smn.uio.no

||Mathias.Bostrom@smn.uio.no

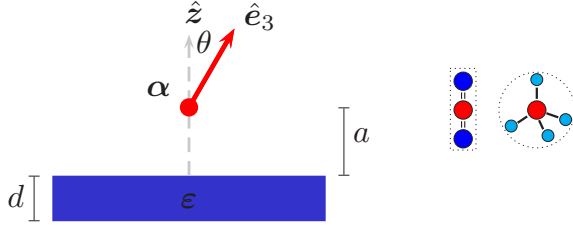


FIG. 1. (Color online) Left: Schematic figure of an anisotropically polarizable molecule above a dielectric slab. Right: Schematic figure showing the anisotropy of the CO₂ molecule and the isotropy of the CH₄ molecule in their polarizabilities.

II. FORMALISM

Consider an anisotropically polarizable molecule described by a frequency dependent molecular polarizability

$$\alpha(\omega) = \alpha_1(\omega)\hat{\mathbf{e}}_1\hat{\mathbf{e}}_1 + \alpha_2(\omega)\hat{\mathbf{e}}_2\hat{\mathbf{e}}_2 + \alpha_3(\omega)\hat{\mathbf{e}}_3\hat{\mathbf{e}}_3, \quad (1)$$

at a distance a above an anisotropically polarizable dielectric slab of thickness d . The dielectric slab is described by dielectric permittivity

$$\epsilon(\omega) = \epsilon^\perp(\omega)\mathbf{1}_\perp + \epsilon^\parallel(\omega)\hat{\mathbf{z}}\hat{\mathbf{z}}, \quad (2)$$

where \perp components are in the x - y plane containing the dielectric slab and the \parallel component is normal to the surface of the slab (see Fig. 1). For an isotropic material such as amorphous silica, we can set $\epsilon^\perp = \epsilon^\parallel$. Magnetic permeabilities for both the molecule and the dielectric slab are set to 1.

Here, the principal axes of the molecule are

$$\hat{\mathbf{e}}_1 = \cos\beta\hat{\boldsymbol{\theta}} + \sin\beta\hat{\boldsymbol{\phi}}, \quad (3a)$$

$$\hat{\mathbf{e}}_2 = -\sin\beta\hat{\boldsymbol{\theta}} + \cos\beta\hat{\boldsymbol{\phi}}, \quad (3b)$$

$$\hat{\mathbf{e}}_3 = \hat{\mathbf{r}}, \quad (3c)$$

where β is the rotation about the unit vector $\hat{\mathbf{e}}_3$, and $\hat{\mathbf{r}}$, $\hat{\boldsymbol{\theta}}$, and $\hat{\boldsymbol{\phi}}$ are the unit vectors in the spherical polar coordinates,

$$\hat{\mathbf{r}} = \sin\theta\cos\phi\hat{\mathbf{x}} + \sin\theta\sin\phi\hat{\mathbf{y}} + \cos\theta\hat{\mathbf{z}}, \quad (4a)$$

$$\hat{\boldsymbol{\theta}} = \cos\theta\cos\phi\hat{\mathbf{x}} + \cos\theta\sin\phi\hat{\mathbf{y}} - \sin\theta\hat{\mathbf{z}}, \quad (4b)$$

$$\hat{\boldsymbol{\phi}} = -\sin\phi\hat{\mathbf{x}} + \cos\phi\hat{\mathbf{y}}. \quad (4c)$$

Our configuration with an anisotropic molecule above a dielectric slab with isotropic polarizability in the x - y plane renders the interaction energy independent of ϕ . The interaction energy, neglecting quadrupole and higher moments, at zero temperature in the Fourier transformed space is

$$E = -\hbar c \int_{-\infty}^{\infty} \frac{d\zeta}{c} \int_0^{\infty} \frac{k_\perp dk_\perp}{2\pi} \int_0^{2\pi} \frac{d\phi_k}{2\pi} \frac{e^{-2\kappa a}}{2\kappa} I(i\zeta), \quad (5)$$

which is a generalization of the result given in Ref. [21]. The details of the derivation leading to Eq. (5) has been omitted for brevity. Here,

$$I(i\zeta) = r^H [k^2(\hat{\mathbf{k}}_\perp \cdot \boldsymbol{\alpha} \cdot \hat{\mathbf{k}}_\perp) + k_\perp^2(\hat{\mathbf{z}} \cdot \boldsymbol{\alpha} \cdot \hat{\mathbf{z}})] - r^E \zeta^2 [(\hat{\mathbf{z}} \times \hat{\mathbf{k}}_\perp) \cdot \boldsymbol{\alpha} \cdot (\hat{\mathbf{z}} \times \hat{\mathbf{k}}_\perp)]. \quad (6)$$

The particular choice of $(\hat{\mathbf{k}}_\perp, \hat{\mathbf{z}} \times \hat{\mathbf{k}}_\perp, \hat{\mathbf{z}})$ basis facilitates separation of TM (transverse magnetic) and TE (transverse electric) modes. Specifically,

$$\hat{\mathbf{k}}_\perp = \cos\phi_k\hat{\mathbf{x}} + \sin\phi_k\hat{\mathbf{y}}, \quad (7a)$$

$$\hat{\mathbf{z}} \times \hat{\mathbf{k}}_\perp = -\sin\phi_k\hat{\mathbf{x}} + \cos\phi_k\hat{\mathbf{y}}. \quad (7b)$$

r^H and r^E are the reflection coefficients for TM and TE modes:

$$r^H = -\left(\frac{\bar{\kappa}^H - \kappa}{\bar{\kappa}^H + \kappa}\right) \frac{(1 - e^{-2\kappa^H d})}{\left[1 - \left(\frac{\bar{\kappa}^H - \kappa}{\bar{\kappa}^H + \kappa}\right)^2 e^{-2\kappa^H d}\right]}, \quad (8a)$$

$$r^E = -\left(\frac{\kappa^E - \kappa}{\kappa^E + \kappa}\right) \frac{(1 - e^{-2\kappa^E d})}{\left[1 - \left(\frac{\kappa^E - \kappa}{\kappa^E + \kappa}\right)^2 e^{-2\kappa^E d}\right]}, \quad (8b)$$

where

$$\kappa^H = \sqrt{k_\perp^2 \frac{\epsilon^\perp}{\epsilon^\parallel} + \frac{\zeta^2}{c^2} \epsilon^\perp}, \quad \bar{\kappa}^H = \frac{\kappa^H}{\epsilon^\perp}, \quad (9a)$$

$$\kappa^E = \sqrt{k_\perp^2 + \frac{\zeta^2}{c^2} \epsilon^\perp}, \quad \kappa = \sqrt{k_\perp^2 + \frac{\zeta^2}{c^2}}. \quad (9b)$$

The interaction energy after performing the ϕ_k integration is

$$E = -\hbar c \int_{-\infty}^{\infty} \frac{d\zeta}{c} \int_0^{\infty} \frac{k_\perp dk_\perp}{2\pi} \frac{e^{-2\kappa a}}{2\kappa} \left\{ k_\perp^2 r^H \alpha_3 + \left(\frac{\zeta^2}{c^2}(r^H - r^E) + k_\perp^2 r^H\right) \left(\frac{\alpha_1 + \alpha_2}{2}\right) + \frac{1}{2} \left(\frac{\zeta^2}{c^2}(r^H - r^E) - k_\perp^2 r^H\right) \times \left[\alpha_3 - \frac{\alpha_1 + \alpha_2}{2} + \left(\frac{\alpha_2 - \alpha_1}{2}\right) \cos 2\beta\right] \sin^2 \theta \right\}, \quad (10)$$

where we have suppressed the frequency dependence. The orientation dependence appears only in the last term, which vanishes for $\theta = 0$ and π .

A. Validity of weak approximation

The energy calculated in Eq. (10) is valid in the weak approximation, which was described in [21,22]. The validity of the weak approximation is decided by convergence of the series of the logarithm in the multiple scattering formula for the interaction energy. This series is in essence captured by defining an effective polarizability of an atom above the plate [10]

$$\alpha_{\text{eff}} = \alpha - \frac{1}{2} \boldsymbol{\alpha} \cdot \boldsymbol{\Gamma} \cdot \boldsymbol{\alpha} + \dots, \quad (11)$$

where $\boldsymbol{\Gamma}$ is Green's dyadic for the dielectric slab [21] and $\boldsymbol{\alpha}$ is the atomic polarizability defined in Eq. (1). To get an estimate of the validity of our approximation we note that at low frequencies the TM mode dominates

$$\boldsymbol{\Gamma} \sim \frac{1}{16\pi a^3} \frac{\epsilon - 1}{\epsilon + 1}, \quad (12)$$

where $(\epsilon - 1)/(\epsilon + 1) \approx 1$ at low frequency. Our approximation involves keeping only the first term in Eq. (11), which is

valid if

$$\left(\frac{\alpha}{16\pi}\right)^{1/3} \sim a. \quad (13)$$

For a typical value of the atomic polarizability used in this paper, $\alpha \sim 4 \text{ \AA}^3$, we can check that the separation distance should be larger than 0.4 \AA . However, the continuum picture is not valid at such short distances. Consequently, we would only expect our result to be meaningful at distances above some angstroms, or $\zeta_n > 0.1$. (1 a.u. corresponds to 100 \AA).

B. Perfect conductor limit

In the retarded (Casimir-Polder) regime, the molecular polarizability gets contribution from its static value at zero frequency. The perfect conductor limit ($r^H \rightarrow 1$ and $r^E \rightarrow -1$) in this retarded regime reproduces the known result for the Casimir-Polder energy between an anisotropic molecule and a perfectly conducting slab:

$$E = -\hbar c \frac{\alpha_1 + \alpha_2 + \alpha_3}{8\pi a^4}, \quad (14)$$

where the last term in Eq. (10) uniformly integrates to zero. Thus, in this case the orientation of the molecule has no effect on the interaction energy.

C. Temperature dependence

To account for the temperature (T) dependence, we simply replace the integration over imaginary frequencies by a summation over discrete Matsubara frequencies ζ_n [26,27],

$$E = -2k_B T \sum_{n=0}' \int_0^\infty dk_\perp k_\perp \frac{e^{-2\kappa a}}{2\kappa} I(i\zeta_n), \quad (15)$$

where $\zeta_n = 2\pi n k_B T / \hbar$, k_B is the Boltzmann constant, and the prime indicates that the $n = 0$ term should be divided by 2. $I(i\zeta_n)$ is given by Eq. (6), with ζ replaced by ζ_n .

D. Nonretarded limit

In the nonretarded London-van der Waals limit $\zeta_c a \ll 1$, where ζ_c is some characteristic frequency of the polarizability or permittivity, we can omit the frequency dependence except in the material properties. Then, the finite temperature interaction energy between an anisotropic molecule at a distance a above an isotropic half-space Eq. (10) turns out to be

$$E^{NR} = -2k_B T \sum_{n=0}' \int_0^\infty dk_\perp k_\perp^2 \Delta e^{-2k_\perp a} \left\{ \alpha_3 + \left(\frac{\alpha_1 + \alpha_2}{2}\right) - \frac{1}{2} \left[\alpha_3 - \frac{\alpha_1 + \alpha_2}{2} + \left(\frac{\alpha_2 - \alpha_1}{2}\right) \cos 2\beta \right] \sin^2 \theta \right\}, \quad (16)$$

using $r^H \rightarrow \Delta = (\varepsilon - 1)/(\varepsilon + 1)$ and $r^E \rightarrow 0$, where Δ and α_i are functions of $\zeta_n = 2\pi n k_B T / \hbar$. This energy is proportional to $1/a^3$.

III. DIELECTRIC FUNCTION AND POLARIZABILITY

All calculations for amorphous silica were carried out using the Vienna *ab initio* simulation package (VASP) with the Perdew-Burke-Ernzerhof (PBE) [28] functional. Projector augmented wave pseudopotentials [29,30] were used to model the effect of core electrons. The nonlocal parts of the pseudopotentials were treated in the real space for the Born-Oppenheimer molecular dynamics (BOMD) and in the reciprocal space for all other DFT calculations. The structure of amorphous silica was generated using the BOMD simulations of a 72-atom supercell with different annealing-quenching temperature protocols similar to earlier studies [31,32]. The dielectric properties of amorphous silica were then calculated using the scissors-operator approximation ($\Delta = 3.6$) for PBE calculations. The dielectric function on the imaginary frequency axis was determined using the Kramers-Kronig dispersion relation. The low-energy spectra are verified by calculating the static dielectric constants from the Born effective charges. The static dielectric constant was found to be 4.08 ± 0.11 . The details of the calculations of anisotropic dielectric functions for gold sheets were presented by Bostrom *et al.* in Ref. [23]. We plot the parallel and perpendicular dielectric constants as defined in Eq. (2) of different thicknesses of gold films, and of amorphous silica in Fig. 2.

The anisotropic polarizability tensors at imaginary frequencies for CO_2 and CH_4 were calculated using the quantum chemistry package MOLPRO [33]. Calculations were performed at the coupled clusters, singles and doubles (CCSD) level of theory. The correlation-consistent aug-cc-pVQZ basis set [34] was used. The geometries of the molecules were first optimized by energy minimization before being used in polarizability calculations. All calculations were done at room temperature. The polarizabilities were calculated in free space. It is plausible

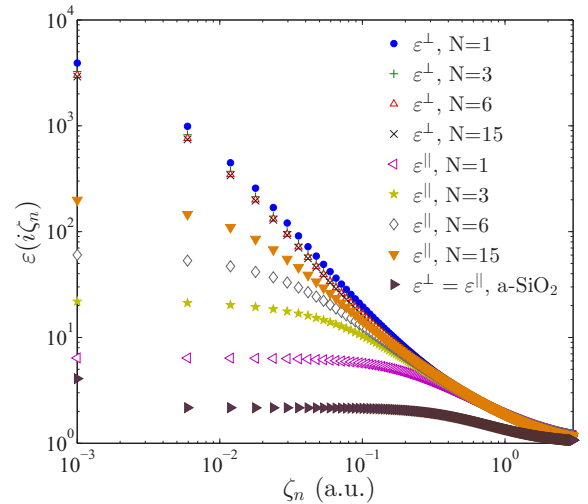


FIG. 2. (Color online) The perpendicular and parallel dielectric constants for $N = 1, 3, 6,$ and 15 atomic layers of gold, and for an amorphous silica slab (written as a-SiO₂ in the figure) in terms of the Matsubara frequencies. The perpendicular components of the 3-, 6-, and 15-atomic-layer-thick gold films almost overlap. The dielectric constants at zero frequency are shown on the y axis. 1 a.u. = $6.57968 \times 10^{15} \text{ Hz} = 27.212 \text{ eV}$.

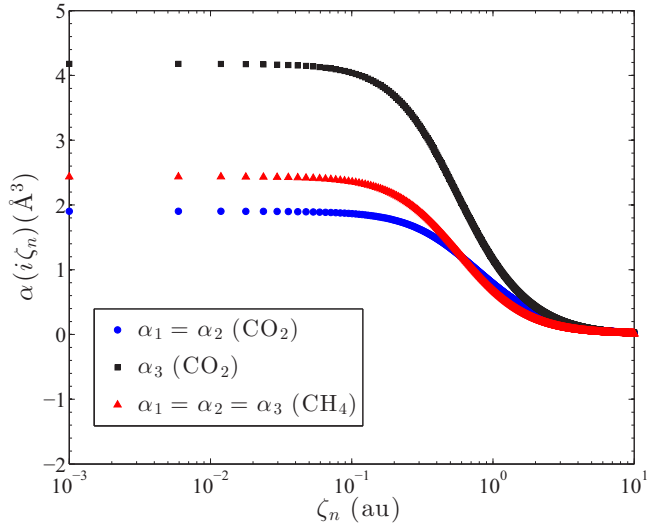


FIG. 3. (Color online) The anisotropic polarizabilities of CO₂ and CH₄ in units of Å³ in terms of the Matsubara frequencies. The zero frequency polarizabilities are indicated on the y axis. Note that CO₂ is much more polarizable in the parallel direction.

that proximity to a surface may induce some distortion of the electron cloud of the molecule, introducing a degree of anisotropy into the dipolar polarizability. The degree of any such surface-induced anisotropy is likely to be small compared with the native anisotropy found in molecules such as CO₂. This is supported by the estimate given in Sec. II A. We show the anisotropic polarizabilities of CO₂ and CH₄ molecules in Fig. 3.

IV. NUMERICAL RESULTS

For a linear molecule such as CO₂, the two most notable configurations are the parallel and perpendicular orientations with respect to the dielectric slab, and we are interested in the change in interaction energies in going from one orientation to the other. By parallel orientation, we refer to the configuration in which $\hat{\mathbf{e}}_3$ is aligned along $\hat{\mathbf{z}}$, while perpendicular orientation refers to the case when they make an angle $\theta = \pi/2$. A CO₂ molecule has anisotropy in one direction in its diagonal basis as shown in Fig. 3. Thus, choosing $\hat{\mathbf{e}}_3$ along the unique linear axis of the molecule, it is obvious from Eq. (10) that there is no β dependent term in the interaction energy. In this particular choice of axes, the unique linear axis of the CO₂ molecule is perpendicular to the surface when $\theta = 0$ (parallel orientation) and parallel to the surface when $\theta = \pi/2$ (perpendicular orientation). The curves in Fig. 4 show the Casimir-Polder interaction energies of a CO₂ and a CH₄ molecule for different θ orientations placed at a distance of 10 Å from an amorphous silica slab. As expected, a methane molecule being highly isotropic shows no change in energy with change in θ . A CO₂ molecule, on the other hand, exhibits a slight change in the interaction energy at different orientations. The curve in Fig. 4 shows that the CO₂ molecule has lower energy at the parallel orientation ($\theta = 0$) than at the perpendicular orientation ($\theta = \pi/2$) near an amorphous silica slab. Thus, the molecule is most stable when its unique linear axis is aligned

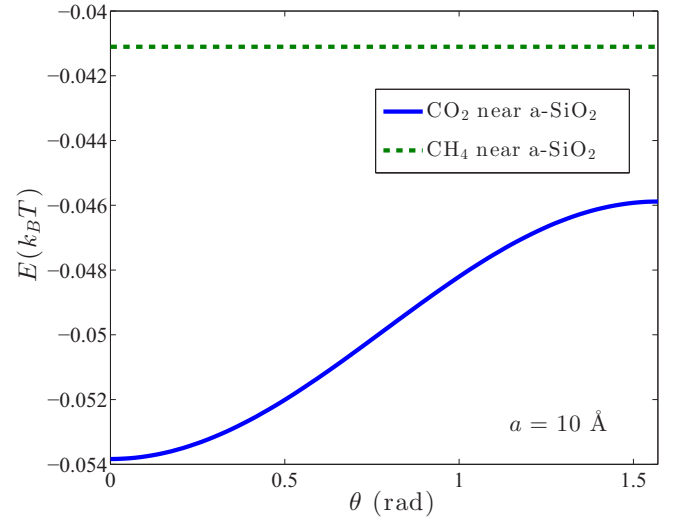


FIG. 4. (Color online) Comparing the interaction energies of CO₂ and CH₄ molecules at a distance of 10 Å from an amorphous silica slab with respect to θ orientation. We refer to the configuration $\theta = 0$ as the parallel orientation and $\theta = \pi/2$ as the perpendicular orientation. All energies are in units of $k_B T$.

perpendicular to the slab. Irrespective of their orientations, the magnitude of the energy is larger for a CO₂ molecule than for a CH₄ molecule. These interaction energies are, however, very small compared to $k_B T$. They become comparable when the molecule is very near the surface (see insets of Figs. 6 and 7). It should be noted that the dielectric continuum picture of our model breaks down at the small distance limit (roughly below 10 Å). A more rigorous quantum chemistry calculation will be required to take into account the effects due to surface, bonding, etc.

To make an estimate within our model with regard to the observed preference of CO₂ over CH₄ molecules in surface adsorption, we calculate the energy of a system consisting of an amorphous silica slab with CO₂ molecules in the parallel orientation at, say, 8 Å and CH₄ molecules at, say, 5 Å from the slab mimicking the condition when the CO₂ gas is being injected. We then consider the reverse system when the CO₂ molecules are at 5 Å and CH₄ molecules at 8 Å. The difference in the interaction energies between the two configurations is $0.078k_B T$, which is roughly 18% compared to the energy in the first configuration. Thus, the second system with CO₂ near the surface is more favorable. As stated earlier, at such small separation distances there would be considerable contributions to the interaction energy from other effects.

In Fig. 5, we plot curves for the variation of molecule-surface interaction energy with respect to θ for a CO₂ molecule near gold films of different thicknesses. As can be observed from the figure, thicker films give larger magnitudes of interaction energies. Only the interaction energy with the one-atomic-layer-thick gold film displays appreciable difference in comparison with the energy curve for $N = 15$ atomic-layer-thick gold film while the interaction energies with the three and six-atomic-layer-thick gold films gradually approach that of 15-atomic-layer-thick gold film. From Figs. 4 and 5, we can see that the trends of the energy curves are alike but the molecules have energies larger in magnitude for a gold

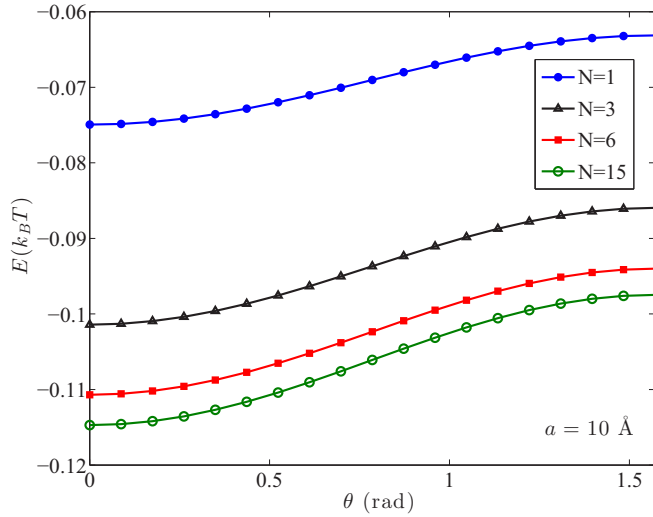


FIG. 5. (Color online) Interaction energies in units of $k_B T$ of a CO_2 molecule for different θ orientations near gold films of N -atomic-layer thickness. The corresponding energies for a CH_4 molecule are -57.9 , -77.8 , -84.8 , and -87.8 in units of $10^{-3}k_B T$ for $N = 1, 3, 6$, and 15 , respectively.

film compared to the $100\text{-}\text{\AA}$ -thick amorphous silica. We also provide the corresponding energies for a CH_4 molecule near gold films of varying thickness in the caption of Fig. 5.

In Fig. 6, we fix the CO_2 molecule in the parallel and perpendicular orientations and plot the interaction energy with respect to separation distance from the amorphous silica slab on a logarithmic scale. The energy curve for CH_4 , which is orientation independent, is also shown. A small difference in the energy curves for the parallel and perpendicular orientations is observed for a CO_2 molecule. The interaction energy is larger

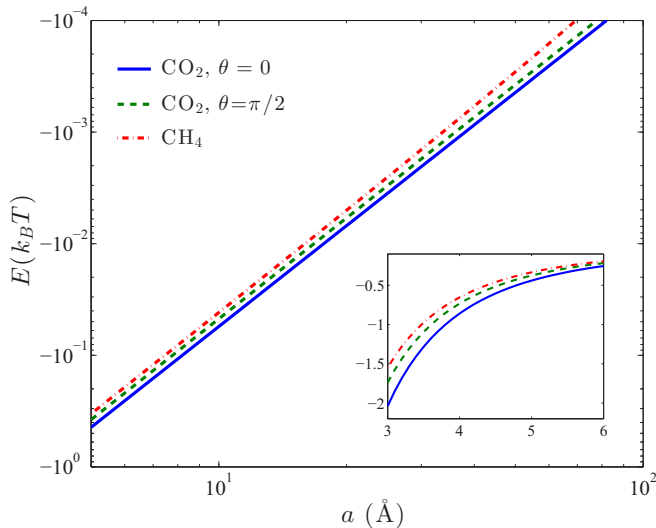


FIG. 6. (Color online) Comparing the interaction energies (in units of $k_B T$) of CH_4 and CO_2 molecules at the parallel ($\theta = 0$) and the perpendicular ($\theta = \pi/2$) orientations at a varying distance from an amorphous silica slab. The interaction energy for a methane molecule is independent of θ orientation. The inset figure shows the small distance limit. The axis labels and the legends of the outer figure hold for the inset figure as well.

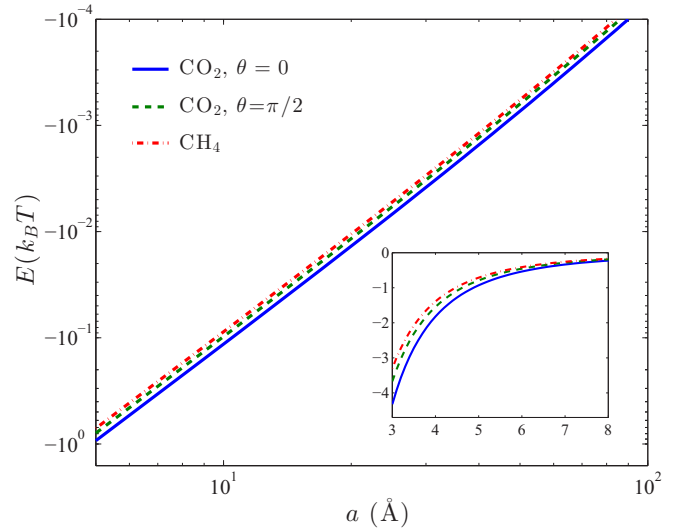


FIG. 7. (Color online) Same as in Fig. 6, but for a 15-atomic-layer-thick gold film.

in magnitude for a CO_2 molecule than for a CH_4 molecule at all separation distances from the slab owing to greater polarizabilities of a CO_2 molecule. The curves follow the $1/a^3$ dependence of the nonretarded approximation (16) up to a separation distance of a few angstroms, and gradually deviate. The inset figure shows the interaction energy in the small molecule-slab separation distance limit (on a linear scale). Figure 7 shows similar curves near a 15-atomic-layer-thick gold film.

V. CONCLUSIONS

In this work, we present a generalized expression for the interaction energy between a completely anisotropic molecule and a dielectric slab polarizable in the direction perpendicular to the surface. Applying this to the specific case of a linearly polarizable CO_2 molecule and an isotropically polarizable CH_4 molecule, we show that anisotropy influences the van der Waals energy to a small degree. The parallel orientation ($\theta = 0$) is more favored in comparison to the perpendicular orientation ($\theta = \pi/2$) in the case of a CO_2 molecule. In subsequent studies, it will be interesting to incorporate the effects of finite size of the molecule in which one has to carefully consider different radii of the anisotropic molecule in different directions for determination of the interaction energy for different orientations; in other words, go beyond the dipole approximation. Very recently, Bimonte *et al.* pointed out the importance of the role of the curvature of the surface on preferred orientation of the particle [35]. In the future, we hope that it will prove possible to transcend the limitations of the continuum approximation, to get more reliable estimates of Casimir-Polder energies at very short distances than we can provide here.

ACKNOWLEDGMENTS

P.T. gratefully acknowledges support from the European Commission. P.T. also acknowledges the Olle Eriksson's Foundation, Sweden (Grant No. VT-2014-0001) for

supporting a fruitful research visit at the Department of Physics, Southern Illinois University (SIU), Carbondale, USA. P.T. acknowledges SIU for its hospitality. M.B., O.I.M., and C.P. acknowledge support from the Research Council of Norway (Project No. 221469). C.P. acknowledges support

from the Swedish Research Council (Contract No. C0485101). We acknowledge access to HPC resources at NSC through SNIC/SNAC and at USIT through NOTUR. The work of K.A.M. is supported in part by a grant from the Julian Schwinger Foundation.

-
- [1] V. A. Parsegian, *Van der Waals Forces: A Handbook for Biologists, Chemists, Engineers, and Physicists* (Cambridge University Press, Cambridge, 2006).
- [2] F. Capasso, J. N. Munday, D. Iannuzzi, and H. B. Chan, Casimir forces and quantum electrodynamical torques: Physics and nanomechanics, *IEEE J. Select. Top. Quant. Electron.* **13**, 400 (2007).
- [3] A. W. Rodriguez, A. P. McCauley, D. Woolf, F. Capasso, J. D. Joannopoulos, and S. G. Johnson, Nontouching Nanoparticle Diclusters Bound by Repulsive and Attractive Casimir Forces, *Phys. Rev. Lett.* **104**, 160402 (2010).
- [4] Y. Lin, I. Teper, C. Chin, and V. Vuletić, Impact of the Casimir-Polder Potential and Johnson Noise on Bose-Einstein Condensate Stability Near Surfaces, *Phys. Rev. Lett.* **92**, 050404 (2004).
- [5] M. Antezza, L. P. Pitaevskii, and S. Stringari, Effect of the Casimir-Polder force on the collective oscillations of a trapped Bose-Einstein condensate, *Phys. Rev. A* **70**, 053619 (2004).
- [6] M. Kardar and R. Golestanian, The ‘friction’ of vacuum, and other fluctuation-induced forces, *Rev. Mod. Phys.* **71**, 1233 (1999).
- [7] V. V. Dodonov, Current status of the dynamical Casimir effect, *Phys. Scr.* **82**, 038105 (2010).
- [8] C. M. Wilson, G. Johansson, A. Pourkabirian, M. Simoen, J. R. Johansson, T. Duty, F. Nori, and P. Delsing, Observation of the dynamical Casimir effect in a superconducting circuit, *Nature (London)* **479**, 376 (2011).
- [9] P. Lähteenmäki, G. S. Paraoanu, J. Hassel, and P. J. Hakonen, Dynamical Casimir effect in a Josephson metamaterial, *Proc. Natl. Acad. Sci. USA* **110**, 4234 (2013).
- [10] J. S. Hoye, I. Brevik, and K. A. Milton, Casimir friction between polarizable particle and half-space with radiation damping at zero temperature, *J. Phys. A: Math. Theor.* **48**, 365004 (2015).
- [11] J. Tao and A. M. Rappe, Physical Adsorption: Theory of van der Waals Interactions between Particles and Clean Surfaces, *Phys. Rev. Lett.* **112**, 106101 (2014).
- [12] J. F. Babb, Casimir effects in atomic, molecular, and optical physics, *Adv. At. Mol. Opt. Phys.* **59**, 1 (2010).
- [13] K. A. Milton, Resource letter VWCPF-1: van der Waals and Casimir-Polder forces, *Am. J. Phys.* **79**, 697 (2011).
- [14] B. M. Axilrod and E. Teller, Interaction of the van der Waals type between three atoms, *J. Chem. Phys.* **11**, 299 (1943).
- [15] D. P. Craig and E. A. Power, The asymptotic Casimir-Polder potential for anisotropic molecules, *Chem. Phys. Lett.* **3**, 195 (1969).
- [16] D. P. Craig and E. A. Power, The asymptotic Casimir-Polder potential from second-order perturbation theory and its generalization for anisotropic polarizabilities, *Int. J. Quantum Chem.* **3**, 903 (1969).
- [17] O. I. Malyi, P. Thiyam, M. Boström, and C. Persson, A first principles study of CO₂ adsorption on α -SiO₂(001) surfaces, *Phys. Chem. Chem. Phys.* **17**, 20125 (2015).
- [18] D. F. Parsons, V. Deniz, and B. W. Ninham, Nonelectrostatic interactions between ions with anisotropic ab initio dynamic polarizabilities, *Colloids Surf. A: Physicochem. Eng. Aspects* **343**, 57 (2009).
- [19] P. Thiyam, C. Persson, B. E. Sernelius, D. F. Parsons, A. Malthe-Sørensen, and M. Boström, Intermolecular Casimir-Polder forces in water and near surfaces, *Phys. Rev. E* **90**, 032122 (2014).
- [20] P. Thiyam, C. Persson, D. F. Parsons, D. Huang, S. Y. Buhmann, and M. Boström, Trends of CO₂ adsorption on cellulose due to van der Waals forces, *Colloids Surf. A: Physicochem. Eng. Aspects* **470**, 316 (2015).
- [21] P. Parashar, K. A. Milton, K. V. Shajesh, and M. Schaden, Electromagnetic Semitransparent δ -Function Plate: Casimir Interaction Energy between Parallel Infinitesimally Thin Plates, *Phys. Rev. D* **86**, 085021 (2012).
- [22] K. V. Shajesh and M. Schaden, Repulsive long-range forces between anisotropic atoms and dielectrics, *Phys. Rev. A* **85**, 012523 (2012).
- [23] M. Boström, C. Persson, and Bo E. Sernelius, Casimir force between atomically thin gold films, *Eur. Phys. J. B* **86**, 43 (2013).
- [24] D. F. Parsons and B. W. Ninham, Ab initio molar volumes and Gaussian radii, *J. Phys. Chem. A* **113**, 1141 (2009).
- [25] D. F. Parsons and B. W. Ninham, Importance of accurate dynamic polarizabilities for the ionic dispersion interactions of alkali halides, *Langmuir* **26**, 1816 (2009).
- [26] E. M. Lifshitz, The theory of molecular attractive forces between solids, *Zh. Eksp. Teor. Fiz.* **29**, 94 (1955) [*Sov. Phys. JETP* **2**, 73 (1956)].
- [27] J. Mahanty and B. W. Ninham, *Dispersion Forces* (Academic, London, 1976).
- [28] J. P. Perdew, K. Burke, and M. Ernzerhof, Generalized Gradient Approximation Made Simple, *Phys. Rev. Lett.* **77**, 3865 (1996).
- [29] G. Kresse and D. Joubert, From ultrasoft pseudopotentials to the projector augmented-wave method, *Phys. Rev. B* **59**, 1758 (1999).
- [30] P. E. Blöchl, Projector augmented-wave method, *Phys. Rev. B* **50**, 17953 (1994).
- [31] J. Sarnthein, A. Pasquarello, and R. Car, Structural and Electronic Properties of Liquid and Amorphous SiO₂: An *ab initio* Molecular Dynamics Study, *Phys. Rev. Lett.* **74**, 4682 (1995).
- [32] R. M. Van Ginhoven, H. Jönsson, and L. R. Corrales, Silica glass structure generation for *ab initio* calculations using small samples of amorphous silica, *Phys. Rev. B* **71**, 024208 (2005).

- [33] H.-J. Werner, P. J. Knowles, R. Lindh, F. R. Manby, M. Schütz *et al.*, MOLPRO, version 2008.1, a package of ab initio programs, 2008, <http://www.molpro.net>.
- [34] K. A. Peterson and T. H. Dunning, Jr., Accurate correlation consistent basis sets for molecular core-valence correlation effects: The second row atoms Al-Ar, and the first row atoms B-Ne revisited, *J. Chem. Phys.* **117**, 10548 (2002).
- [35] G. Bimonte, T. Emig, and M. Kardar, Casimir-Polder force between anisotropic nanoparticles and gently curved surface, *Phys. Rev. D* **92**, 025028 (2015).